# Microstructural aspects of adiabatic shear failure in annealed Ti6Al4V

P. Landau[1], A. Venkert[2] and D. Rittel[3*]

[1] Department of Materials Engineering, Ben Gurion University, Beer-Sheva, Israel
[2] Department of Physics, NRCN, Beer-Sheva, 84190, Israel
[3] Faculty of Mechanical Engineering, Technion, 32000 Haifa, Israel

Abstract

This work reports a comprehensive examination of the microstructural evolution in Ti6Al4V subjected to high strain rate deformation. The sequence of microstructural re-arrangements leading to adiabatic shear banding is presented. A detailed microstructural comparison between two types of specimens, one that failed by adiabatic shear and the other that was strained to half its failure strain, is carried out. The main observation is that for this material, the microstructure of the two types of specimens is qualitatively identical, indicating that from about half the failure strain until adiabatic shear failure, no additional micro-mechanism is observed to develop and operate. Overall, the microstructure undergoes a significant refinement with the increasing strain until the formation of dynamically recrystallized grains. It is therefore suggested that the evolution of the volume fraction of recrystallized grains should be characterized, from its early onset until final failure by adiabatic shear banding.

Keywords: Ti alloys; shear bands; microstructure; dynamic recrystallization; transmission electron microscopy

(*) Corresponding author: *merittel@technion.ac.il*

## 1. Introduction

Adiabatic shear failure (ASB) is a dynamic failure mechanism that occurs in many ductile materials subjected to impact loading. The characteristic feature of this mechanism is the development of a narrow band or plane (adiabatic shear band, subsequently referred to as ASB) in which very large local strains and high temperatures prevail, resulting in uncontrolled failure [1, 2].

ASB has been traditionally linked to thermally induced strain softening leading to a loss of stability of the plastic deformation [3-5]. While a profusion of reports on microstructural aspects of ASB can be found (for a review, see e.g.[6]), coordinated mechanical-microstructural experiments on this subject are still very scarce. Recently, Rittel et al. [7] proposed to re-analyze the onset of adiabatic shear banding in terms of the dynamically stored energy of cold work in the material. Being an energetic concept, the latter connects naturally to microstructural re-arrangements occurring in the material during the dynamic process. In parallel, one finds a very large number of reports of dynamic recrystallization observed in the broken ASB in numerous metals [6, 8-16]. This observation is again justified in terms of the high temperature inside the band. A contradictory observation was reported by Rittel et al. [17] for annealed Ti6AL4V, where the authors observed dynamically recrystallized (DRX) grains in specimens that had not failed and were only loaded to roughly half their failure strain by ASB. This striking observation showed that, contrary to the common belief, DRX actually precedes ASB rather than being its consequence. A related suggestion was that DRX is in fact driven by the dynamically stored energy of cold work which acts as the thermodynamic driving force of the process. Yet, two central issues remain open, namely:

1. What is the sequence of microstructural re-arrangements leading to ASB?
2. What are the kinetics of the DRX growth until a full ASB is formed?

The first issue is principally addressed in this paper. Specifically, the microstructure of the specimens used in [17] is analyzed in great detail in order to pinpoint the microstructural resemblances and differences between failed and deformed specimens. The idea is that, since the locus for ASB formation is identified a-priori as the fillet of the gauge section (stress-concentration), the microstructure can be systematically characterized as a function of the distance from the fillet, revealing the various degrees to which it evolves. Based on this approach, both failed and partially deformed (interrupted) specimens can be characterized and compared since the failure locus is well defined, as discussed in the sequel, whether as a potential or actual fracture plane.

Extensive research has been devoted to the microstructural evolution in shear localization areas. A recent extensive review by Xu et. al. [6] summarized the microstructural evolution related to

adiabatic shear localization for strain rates of $10^3$-$10^4 s^{-1}$in various metals including Ti and its alloys. The primary metallurgical process occurring during high strain rate deformation is believed to be dynamic recovery in the form of dislocation cell formation, similar to the microstructural evolution of metals subjected to severe plastic deformation [18]. Evolution here is to be understood as strain-related rather than the usual temporal implication. As the ASB is approached, the elongated dislocation cells break down and are gradually replaced by small new grains. The microstructural evolution consists therefore of a noticeable refinement ending in dynamic recrystallization (DRX). A few mechanisms for high strain rate DRX have been proposed [8, 11]. The sequence of events is mainly described as a process of continuous (rotational) DRX where, while deformation proceeds and the shear band is approached, the degree of misorientation increases. The process ultimately ends in the formation of new nano/micrograins [6, 9, 19-22].

As mentioned before, an abundant literature is available on the microstructural evolution of different alloys with the recurring observation, irrespective of the investigated material, of dynamic recrystallization taking place in the adiabatic shear band [11], as evidenced from very small (a few tens on nanometers) grains with a very low dislocation density, indicating a soft undeformed material. DRX is therefore intimately associated with adiabatic shear failure with its characteristic large strains and temperatures, although the phenomenon has been shown to be athermal, occurring even at cryogenic temperatures (see e.g. [8]).

Ti6Al4V alloy is one of the most attractive engineering alloys due to its low density, high specific strength, resistance to corrosion and good high temperature properties. The selected material for this study is annealed Ti6Al4V alloy which possesses a marked propensity to fail by ASB formation [1, 4, 12, 23, 24] A brief literature survey follows in order to summarize the latest developments on microstructural aspects of dynamic failure of this and related alloys.

The microstructural aspects of ASB formation in Ti6Al4V were mainly studied following high strain rate deformation in the form of ballistic impact and shock loading [12, 15, 24-26], where the typical strain rates were $\dot{\varepsilon} \geq 10^4\, s^{-1}$. Transmission electron microscopy (TEM) observations revealed that at these strain rates, DRX is found within the ASB in the form of a few tens of nanometer diameter grains located in a high dislocation density matrix. Lee and Lin [27] investigated this alloy at a lower strain rate ($\dot{\varepsilon}=10^3\, s^{-1}$) over a large range of temperatures. These authors presented limited microstructural information using transmission electron microscopy, with emphasis on dislocation cells' structure at various temperatures. The majority of the work performed in the $\dot{\varepsilon}=10^3-10^4\, s^{-1}$ range concerned $\alpha$-Ti [16, 28, 29]. The microstructural evolution following high strain rate deformation was found to be similar to that of other metals and alloys which are susceptible to shear

band formation, namely formation of dislocation cells, subgrains and DRX. Altogether, all the characterized materials bear a common overall microstructural evolution. However, the microstructural evolution in the vicinity of the ASB and within it was not fully reported for Ti6Al4V to the best of our knowledge.

At this stage, it is important to note that shear band observations are inherently carried out in a high strain gradient area. Therefore, by systematically varying the distance of observation from the shear band (fracture plane) itself, various strain levels are in fact interrogated with their corresponding typical microstructure. What has not been carried out is the same kind of systematic observations, comparing now fully fractured and interrupted specimens [17] from a microstructural point of view. Such a comparison provides a qualitative comparative picture of the kinetics of microstructural refinement.

In this work, a comprehensive examination of the microstructural evolution in dynamically deformed and fractured annealed Ti6Al4V is presented, and the sequence of microstructural re-arrangements leading to ASB is characterized. This work completes and sheds additional light on the preliminary report of Rittel et al. [17] in which the emphasis was mainly put on DRX. The main outcome of the present work is that the microstructure of interrupted specimens – deformed to about half of the failure strain in this case – is qualitatively similar to that of fractured specimens, to a point where they cannot be distinguished. This point is thoroughly developed in this paper.

## 2. Experimental procedure

Shear compression specimens (SCS) were machined from a commercially annealed Ti6Al4V 12.7 mm diameter rod. The SCS is a specimen in which the kinematics of the deformation enforces a shear dominant situation in the gauge section, with homogeneous strain and stress fields [30-32]. The specimen shown in Figure 1 consists of a 10 mm diameter cylinder with a pair of diametrically opposed grooves, making an angle of 45º with respect to the longitudinal axis, which delineates the deforming gauge section of the specimen. As with any non-smooth specimen, a mild state of stress concentration develops in the root of the 2 pairs of fillets (F in Figure 1) that define the gauge section [30], so that adiabatic shear bands *always initiate* in this region of the gauge providing a well defined initiation site. Dynamic tests were carried out at a typical strain rate of $\dot{\varepsilon}=3000\,\mathrm{s}^{-1}$ using a Kolsky (Split Hopkinson pressure bar) apparatus [33] and SCS specimen with a 1.5 mm gauge height, as reported in [17]. The dynamic tests consisted of either impacting specimens until failure (fracture) by ASB formation, or bringing it to a controlled level of strain using hardened steel stop-rings, followed

by elastic unloading. The stop ring ensures that the specimens are impacted only once, as opposed to being repeatedly pounded by the stress waves trapped in the bars. For these specimens, the normalized strain (with respect to fractured specimens), was approximately 0.45. Additional experiments were carried out quasi-statically, in which the specimens were deformed to a normalized strain of the approximate same magnitude, and unloaded without failure, for comparison purposes.

Transmission electron microscopy (TEM) specimens were prepared from each type of specimens (interrupted static, interrupted dynamic and dynamically failed) for a comparative characterization of the microstructure. The specimens were extracted from the fillet region of the specimen, which in the case of fracture, contained the shear band. In addition, the initial microstructure of the undeformed material was characterized in order to provide a reference microstructural state. In the deformed samples, the areas set for observation in all specimens included the fracture plane, whether potential or actual, in order to allow for comparative characterization.

For all the unbroken samples, the electron-transparent area was prepared by jet electro-polishing (Tenupol©) in a solution of 80% Methanol and 20% $HNO_3$. For the fractured samples, the transparent area for electrons was prepared by precision ion polishing (Gatan PIPS). The two preparation methods yielded representative TEM specimens. However, ion milling was the only feasible way to prepare transparent area from the fracture plane itself.

## 3. Results

### *3.1 Mechanical behavior*

The results of the mechanical tests can be found in Rittel et al. [17] and will only be briefly reminded here. As mentioned above, two kinds of tests were performed, namely up to fracture and interrupted before fracture. Dynamic fracture by ASB formation occurred at a strain level of $\varepsilon_f \approx 0.23$ while the deformed specimens that did not fail (subsequently referred to as interrupted tests) reached a level of $\varepsilon_f \approx 0.12$ (normalized $\varepsilon_n \approx 0.45$) at a strain rate of $\dot{\varepsilon} = 3000\,s^{-1}$. In addition, a static interrupted test was carried out up to $\varepsilon_f \approx 0.17$ (normalized $\varepsilon_n \approx 0.68$) to allow for comparison with its dynamic counterpart. Here, it is important to note that the investigated alloy experiences a very small temperature rise prior to the strain-softening phase [23]. Therefore, for the interrupted test cases, the evolution of heat is even smaller so that thermal factors in this case can be ruled out.

### *3.2 Microstructural evolution*

The microstructural evolution of Ti6Al4V was examined using transmission electron microscopy in the vicinity of the shear concentration area, when the field of view was gradually shifted towards the

areas of the fracture plane (ASB). The observations were performed over a distance of a few tens of microns for all the samples, and the results will be presented for each sample starting far away from the shear concentration area, then gradually approaching it (including eventual fracture) for the relevant specimens.

### 3.2.1 Initial microstructure- reference samples

The initial microstructure of annealed Ti6Al4V alloy consists of α and β phases that are readily identified using selected area diffraction patterns (SADP). The α phase grain size is of the order of a 5-10μm while the β phase grain size is finer, of the order of 1μm. The grains are essentially free of dislocations, without noticeable twins or martensitic platelets. Figure 2 shows the typical microstructure of the annealed alloy, where both phases are shown and denoted in the micrograph. A corresponding selected area diffraction pattern of the β phase is attached to the micrograph.

### 3.2.2 Interrupted static specimens

The microstructure of the interrupted sample, in the shear concentration area consists mainly of equiaxed dislocation cells in the α phase, approximately 2 μm in diameter (Figure 3). The interior of the cells contains dislocations, consistent with observations of low strain quasi-static deformation of high stacking fault energy metals [18]. The cell walls consist of tangled dislocations which are also typical of low strains microstructures. The microstructure observed in the interrupted static samples is shown in figure 3a. The attached corresponding selected area diffraction pattern is identified as α phase, with a small misorientation angle between the dislocation cells.

Martensitic platelets are occasionally observed in the β phase, such as those arrowed in Figure 3b. These platelets were identified from the corresponding SADP (attached to the micrograph) as α" (orthorhombic) type, which forms as a result of external stress (i.e. stress-induced martensite) or quenching from high temperature β phase [34, 35].

Overall, the microstructure of the interrupted static samples is consistent with that observed at low strains in many high stacking fault energy metals. At these strains the microstructure consists essentially of dislocation cells that decrease in size and increase in relative misorientation as the strain increases. When moving further towards the shear concentration area, no significant change was observed in the microstructure, even in the fillet edges.

### 3.2.3 Interrupted dynamic specimens

Away from the potential fracture plane (~50μm), the microstructure consists of dislocation cells in the α phase (Figure 4a). The cell size is approximately 2μm, similar to the cell size observed in the interrupted static samples (compare Figure 4a with Figure 3a). Closer to the potential fracture plane (about 10-20μm), the cell walls become sharper, indicating that the dislocation density in the boundaries is higher, and the misorientation angle between adjacent cells is larger than before. The density of martensitic platelets was observed to increase gradually as one gets closer to the shear concentration area (potential fracture plane). In addition, the density of martensitic platelets in the β phase is sensibly higher in the interrupted dynamic samples than in the interrupted static ones (compare Figure 4a with Figure 3a).

As a general remark, note that two types of martensite were observed in the specimens, irrespective of the strain rate. For example: the martensite in Figure 4b is of the α' (hcp) type, which is also stress induced from the β phase, as was the α" (orthorhombic, Figure 3b).

Closer to the stress concentration fillet (potential fracture plane), the detailed internal structure of the cell walls which is revealed by tilting the sample, is shown in Figure 5. The cell walls consist of arrays of parallel dislocations, i.e. dislocation networks (square or hexagonal). These dislocation walls introduce a misorientation between adjacent cells, as can be seen in the corresponding SADP, attached to the micrograph manifested by arc-like reflections. Such arrays of parallel dislocations were neither observed in the interrupted static nor in the current interrupted dynamic samples in areas that are far away (more than 50μm) from the fracture plane. The formation of dislocation networks corresponds to work hardening of the material in the shear localization area.

Closer to the potential facture plane (<10μm), densely packed dislocations or avalanched dislocation cells are observed (Figure 6). Microstructural features such as well-defined dislocation cells or martensitic platelets are no longer distinguishable. However, SADP's clearly reflect a polycrystalline microstructure, i.e. incomplete rings are observed that indicate the presence of dynamically recrystallized nanograins (see for example the attached SADP in Figure 6). Within the avalanched dislocation cells area, several nanograins are directly observed (arrowed in Figure 6). These nanograins are a result of DRX, and they appear to have a very low dislocation density. Nonetheless, these are rather difficult to discern since the high density of the surrounding dislocations screens the new DRX'ed nanograins.

The evolution of the microstructure in the interrupted dynamic samples, approaching the potential fracture plane, can thus be summarized as follows: The cell size decreases, the misorientation angle between cells increases, and the cell boundaries become denser, i.e. the cells become subgrains. As one comes even closer to the potential fracture plane, DRX nanograins are observed within an area comprised of avalanched dislocation cells. The corresponding SADP shows incomplete rings, consistent with DRX, however most of the individual nanograins are screened by the dislocations and are thus hard to resolve (compare Figure 6 and Figure 7c).

### 3.2.4 Dynamically failed specimens

In a similar manner, the microstructural evolution of Ti6Al4V was examined in the shear localization area of fractured samples, where failure due to the formation of ASB had occurred. The fracture plane was located, as expected, in the fillet of the SCS sample.

The evolution of the microstructure in these samples is overall quite similar to the evolution observed in the interrupted dynamic samples. As the field of view is moved closer to the fracture plane, the microstructure changes gradually from dislocation cells (small misorientation angles between adjacent cells), into subgrains (higher misorientation angles between subgrains) manifested in the SADP as spotty ring patterns. Figure 7a shows the typical microstructure observed in this region, consisting of misoriented subgrains in the $\alpha$ phase and a high density of stress induced martensite in the $\beta$ phase. In the core of the fracture plane (shear localization area - Figure 7b), a region comprised of avalanched dislocation cells (high density dislocations) is observed, characterized by incomplete rings in the SADP. Dynamically recrystallized nanograins, with a low dislocation density, 10-50nm in diameter, are again observed within the avalanched dislocations region. These DRX nanograins are discernable at higher magnifications as can be seen in Figure 7c (arrowed). Note that a similar evolution was reported by Xue et al. [19-20] for 316L-SS.

To summarize this section, it appears that the evolution of the microstructure in the broken specimens is quite similar to that of the interrupted specimens, to an extent to which one cannot tell the difference between them on a qualitative basis.

## 4. Discussion

The evolution of the microstructure of commercial Ti6Al4V was examined following high strain rate deformation and compared to the static microstructure at a similar strain. The microstructural features observed are presented in a schematic drawing in Figure 8, illustrating microstructural

refinement as the shear localization area is approached, keeping in mind that a large strain gradient is present in this region.

The initial microstructure of the Ti6Al4V consists of $\alpha$ and $\beta$ phases. The microstructure observed in the interrupted static samples is consistent with the microstructure observed following low strain level deformation of high stacking fault energy metals [18]. The microstructure consists mainly of dislocation cells, with a slight mutual misorientation. Stress induced martensite is occasionally observed.

Consistent with many previous observations, a pronounced microstructural refinement is observed as the observation area gets closer to the (potential) fracture plane. Far away from this area, the microstructure consists of dislocation cells, similar to those observed in static specimens. As the fracture zone is approached (higher strains) the microstructure gets refined by increasing the misorientation angle, resulting in subgrains as observed in similar cases for other materials [9, 11, 12, 22, 28, 29]. Furthermore, for interrupted tests at the core of the potential fracture plane, an area with a high density of dislocations or avalanched dislocation cells is observed. No microstructural features are distinguishable, even though the corresponding selected area diffraction patterns indicate recrystallization, in the form of incomplete rings. Nanograins are discernable within the avalanched dislocation cells area. These nanograins have a very low dislocation density, and are a result of dynamic recrystallization in the shear localization area. It seems that the dynamically recrystallized nanograins are screened by the high dislocation density since the SADP undoubtedly corresponds to many orientations in a small volume, consistent with recrystallization.

The dynamically failed samples exhibit essentially the same microstructural evolution. The refinement of the microstructure as the field of view is moved towards the fracture plane displays the same features, namely dislocation cells evolve into subgrains with higher dislocation density within the walls and higher misorientation angles between adjacent volume elements. An avalanched dislocation area is also observed, in which DRX nanograins originate.

In other words, no significant microstructural differences are observed between the two dynamically deformed samples, failed and partially deformed. Dynamically recrystallized grains are clearly observed in the two types of specimens, which is surprising for specimens that were not loaded to failure, and barely reached half of its failure strain (Figure 6) [17]. Moreover, the recrystallized nanograins seem to have an overall similar shape and dimensions in the two investigated specimens.

As a general remark, one should note the scarcity of work in which the microstructure is tied to the mechanical history of the material with emphasis on adiabatic shear failure. Here, one can find a few noticeable references [19, 20, 36, 37]. The authors in [36] presented an analysis of DRX in shear bands, with emphasis of the local texture. These authors show an excellent adequation between their

analysis and the observed texture of adiabatic shear bands in steel, as well Xue et al. [19, 20] for 316L stainless steel. More recently, dynamic recrystallization in ASB's was successfully modeled using numerical techniques [37]. Here, DRX was represented as a thermally activated phenomenon, rather than as a precursor for failure by ASB.

One important result of this study is the microstructural characterization of the gradual evolution that takes place as a function of the local strain, since an inherent gradient exists in the specimen because of strain concentration effects due to the fillet. In other words, one single specimen was shown to comprise a whole range of increasingly finer microstructures with increasing strain. Consequently, a qualitative description of the gradual refinement was given in Figure 8, which is in good agreement with that reported by Xue et al. for 316L stainless steel [19, 20, 22].

In addition, this study presents important new evidence related to adiabatic shear band formation. Essentially, the present work shows that the overall microstructural evolution of annealed Ti6Al4V can be *fully observed* in dynamically interrupted samples that were only deformed to half their failure strain. These qualitative observations do not allow for a distinction between the two types of specimens, interrupted and failed, since *all the microstructural features are already present in the interrupted specimens*. The next and only microstructural evolution that characterizes the dynamically failed samples is the very formation of the adiabatic shear band itself. This formation is believed to be detected in the global mechanical response of the samples (strain softening), and not by any microstructural changes as shown in this work. This observation suggests that, since additional microstructural refinement does not occur past an "incubation phase" during which DRX'ed grains are formed at an early stage, their volume fraction must increase with the ongoing strain until final failure. Consequently, future studies should concentrate on the kinetics of growth of the recrystallized volume fraction of these grains in some quantitative way (question (2) in the introductory section). Specifically, analyses in the spirit of [36, 37] should be carried out, taking into account athermal early generation of DRX, and the fact that at this stage, the microstructure is qualitatively "frozen".

Another outcome of this study is that the same recrystallized grains are observed prior to and after shear localization without any apparent change in shape or dimensions. This seems to contradict the expectation that virgin grains should be highly deformed in the shear band. One could argue, as has been done, that the high temperature and large strains in the shear band promote dynamic recrystallization, or could at least anneal the deformed nanograins, thereby reducing their dislocation density. This might happen through diffusional processes as the shear band cools down to room temperature after failure, although this happens in a relatively short time for which diffusional effects might not be significant.

As a related effect, one would naturally consider hardening related to the well-known Hall-Petch effect. In this context, the work of [38] brings a valuable insight into the high strain rate deformation of nanograined materials. Specifically, for copper, these authors claim that Hall-Petch hardening is expected for all grain-sizes at high strain-rates, as opposed to a potential reverse softening effect at quasi-static strain rates, as a function of the nanograin size. This point remains to be verified experimentally.

Alternatively, one might think of another deformation mechanism, other than involving slip and motion of dislocations. In this case, [10] have suggested a deformation mechanism that is analogous to superplasticity by which deformation proceeds through grain boundary sliding of the nanograins, with little impact on their initial shape, consistent with the present observations. The few observations of the nanograins' shape, prior to and after failure, seem therefore to support this hypothesis.

## 5. Conclusions

The general evolution of the microstructure of dynamically loaded Ti6Al4V specimens has been characterized as a function of the distance from the fracture plane (adiabatic shear band).

The main characteristic of this evolution consists of microstructural refinement from dislocation cells with increasing misorientation until the formation of dynamically recrystallized grains. In that respect, this evolution is quite similar to that reported for many other metals, while focused on a specific annealed Ti6Al4V alloy.

An original observation concerns the comparison between specimens that were deformed to half its failure strain and failed specimens. This comparison shows beyond any doubt that *the two microstructures are very similar*, with the appearance of DRX'ed grains in the interrupted specimens in spite of its limited deformation [17]. Therefore, long before the adiabatic shear band has formed, all the characteristic microstructural features are already present in the specimens. Consequently, the adiabatic shear band must be characterized by a high volume of DRX'ed grains rather than by any new specific feature, a point that was not previously made.

Future work should therefore concentrate on the kinetics of growth of the recrystallized phase in order to devise a quantitative model leading to the prediction of a fully developed shear band.

## References


[1] Bai Y, Dodd B. Shear Localization: Occurrence, Theories, and Applications. Oxford, UK: Pergamon Press, 1992.

[2] Tresca H. Sur la fluidité et l'écoulement des corps solides. Annales du Conservatoire des Arts et Métiers 1879;4.

[3] Zener C, Hollomon JH. Effect of strain rate upon plastic flow of steel J. Applied Phys. 1944;15:22.

[4] Meyers MA. Dynamic Behavior of Materials. New York, NY: J. Wiley and Sons, 1994.

[5] Molinari A, Clifton RJ. Analytical characterization of the shear localization in thermoviscoplastic materials J. Applied Mech. 1987;54:806.

[6] Xu Y, Zhang J, Bai YL, Meyers MA. Shear localization in dynamic deformation: microstructural evolution. Metallurgical and Material Transactions A 2008;39A:811.

[7] Rittel D, Wang ZG, Merzer M. Adiabatic shear failure and dynamic stored energy of cold work. Physical Review Letters 2006;96:075502.

[8] Hines JA, Vecchio KS. Recrystallization kinetics within adiabatic shear bands. Acta Mater. 1997;45: 635.

[9] Perez-Prado MT, Hines JA, Vecchio KS. Microstructural evolution in adiabatic shear bands in Ta and Ta-W alloys. Acta Mater. 2001;49:2905.

[10] Chokshi AH, Meyers MA. The prospects for superplasticity at high strain rates: preliminary considerations and an example. Scripta Metall. and Mater. 1990;24:606.

[11] Meyers MA, Nesterenko VF, LaSalvia JC, Xu YB, Xue Q. Observation and modeling of dynamic recrystallization in high-strain, high strain-rate deformation of metals. J. Phys. IV France Colloq. C3 2000;PR9:51.

[12] Me-Bar Y, Shechtman D. On the adiabatic shear of Ti-6Al-4V ballistic targets. Matls. Sc. and Engng. 1983;58:181.

[13] Pizana C, Esquivel EV, Murr LE, Pina CY, Baquera MT, Anchondo IA, Magness LS. The role of dynamic recrystallization in [001] single-crystal W and W-Ta alloy ballistic rod penetration into steel targets. Journal of Materials Science 2005;40:4849.

[14] Trillo EA, Esquivel EV, Murr LE, Magness LS. Dynamic recrystallization-induced flow phenomena in tungsten-tantalum (4%) [001] single-crystal rod ballistic penetrators.. Materials Characterization 2002;48:407.

[15] Li GA, Zhen L, Lin C, Gao RS, Tan X, Xu CY. Deformation localization and recrystallization in TC4 alloy under impact condition. Materials Science and Engineering A-Structural Materials Properties Microstructure and Processing 2005;395:98.

[16] Chichili DR, Ramesh KT, Hemker KJ. The high-strain-rate response of alpha-titanium: Experiments, deformation mechanisms and modeling. Acta Materialia 1998;46:1025.

[17] Rittel D, Landau P.,Venkert A. Dynamic recrystallization as a potential cause for adiabatic shear failure. Physical Review Letters 2008;101:165501.

[18] Hughes D, Hansen N. High angle boundaries formed by grain subdivision mechanisms Acta Mat. 1997;45:3871.

[19] Xue Q, Gray GT. Development of adiabatic shear bands in annealed 316L stainless steel: Part I. Correlation between evolving microstructure and mechanical behavior. Metallurgical and Materials Transactions a-Physical Metallurgy and Materials Science 2006;37A:2435.

[20] Xue Q, Gray GT. Development of adiabatic shear bands in annealed 316L stainless steel: Part II. TEM studies of the evolution of microstructure during deformation localization. Metallurgical and Materials Transactions a-Physical Metallurgy and Materials Science 2006;37A:2447.

[21] Andrade U, Meyers MA, Vecchio KS, Chokshi AH. Dynamic recrystallization in high strain, high strain rate plastic deformation of copper. Acta Metall. Mater. 1994;42 3183.

[22] Xue Q, Cerreta EK, Gray GT. Microstructural characteristics of post-shear localization in cold rolled 316L stainless steel Acta Mater. 2007;55:691.

[23] Rittel D, Wang ZG. Thermo-mechanical aspects of adiabatic shear failure of AM50 and Ti6Al4V alloys. Mechanics of Materials 2008;40:629.

[24] Timothy SP, Hutchings IM. Initiation and Growth of Microfractures Along Adiabatic Shear Bands in Ti-6Al-4V. Materials Science and Technology 1985;1:526.

[25] Timothy SP, Hutchings IM. The Structure of Adiabatic Shear Bands in a Titanium-Alloy. Acta Metallurgica 1985;33:667.

[26] Xue Q, Meyers MA, Nesterenko VF. Self-organization of shear bands in titanium and Ti-6Al-4V alloy. Acta Materialia 2002;50:575.

[27] Lee WS, Lin CF. High-temperature deformation behaviour of Ti6Al4V alloy evaluated by high strain-rate compression tests. J. Mat. Process. Tech. 1998;75:127.

[28] Meyers MA, Pak HR. Observation of an Adiabatic Shear Band in Titanium by High-Voltage Transmission Electron-Microscopy. Acta Metallurgica 1986;34:2493.

[29] Chichili DR, Ramesh KT, Hemker KJ. Adiabatic shear localization in alpha-titanium: experiments, modeling and microstructural evolution. Journal of the Mechanics and Physics of Solids 2004;52:1889.

[30] Dorogoy A, Rittel D. Numerical validation of the shear compression specimen (SCS). Part I: Quasi-static large strain testing. Exp. Mech. 2005;45:167.

[31] Dorogoy A, Rittel D. Numerical validation of the shear compression specimen (SCS). Part II: Dynamic large strain testing. Exp. Mech. 2005;45:178.

[32] Rittel D, Lee S, Ravichandran G. A shear compression specimen for large strain testing. Experimental Mechanics 2002;42:58.

[33] Kolsky H. An investigation of the mechanical properties of materials at very high rates of loading. Proc. Phys. Soc. London 1949;62-B:676.

[34] Leguey T, Schaublin R, Marmy P, Victoria M. Microstructure of Ti5Al2.5Sn and Ti6Al4V deformed in tensile and fatigue tests. J. Nuc. Mat. 2002;305:52.

[35] Atroshenko SA. Martensite transformation in metals induced shock loading. Mat. Sci. Eng. A 2004;378:293.

[36] Toth LS, Hildenbrand A, Molinari A. Dynamic recrystallisation in adiabatic shear bands. J. de Phys. IV France 2000;10:Pr9.

[37] Medyanik S, Liu W, Li S. On criteria for adiabatic shear band propagation. J.Mech. Phys. Solids 2007;55:1439.

[38] Mercier S, Molinari A, Estrin Y. Grain size dependence of strength of nanocrystalline materials as exemplified by copper: An elastic-viscoplastic modelling approach. J. Matls. Sc. 2007;42:1455.

## Figure Captions

Figure 1: A typical shear compression specimen before (A) and after deformation (B). The block arrows show the applied load direction and the thin arrows point to the stress-concentration fillets (F) where ASB's form. Specimens for transmission electron microscopy were taken from this area.

Figure 2: Reference sample - TEM micrograph: The initial microstructure of annealed Ti6Al4V alloy consists of α and β phases, marked in the micrograph. A β grain is arrowed in the micrograph and a corresponding SADP is attached.

Figure 3: Interrupted static sample – TEM micrograph: (a) The typical microstructure consists of dislocation cells within the α phase. Corresponding SADP of α- Ti is attached to the micrograph (b) Area showing stress-induced (α") martensite (arrowed) transformed from the β phase, and its corresponding SADP.

Figure 4: Interrupted dynamic sample – TEM micrographs far away from the shear concentration area: (a) The typical microstructure consists of dislocation cells in the α phase and a higher density of stress induced martensite in the β phase, both denoted on the micrograph. (b) Area showing stress- induced (α') martensite (arrowed) transformed from the β phase, and its corresponding SADP.

Figure 5: Interrupted dynamic sample - TEM micrograph close to the shear concentration area (about 10-20μm). Detailed internal structure of dislocation cell walls, consisting of square and hexagonal dislocation networks in the α phase. The attached corresponding SADP shows small misorientation angle between adjacent dislocation cells caused by the hexagonal network arrowed in the micrograph.

Figure 6: Interrupted dynamic sample- TEM micrograph in the shear concentration area. Dynamically recrystallized grains formed in the highly dislocated area are indicated by arrows. The size of the grains ranges from 10-30 nm and have a low dislocation density. The corresponding SADP consists of ring patterns, typical of nanograined polycrystalline materials.

Figure 7: Dynamically failed specimen - TEM-micrographs. (a) Far from the ASB: Dislocation cells and stress-induced martensite. The typical SADP mainly contains misoriented α phase cells. (b) Within the ASB: High dislocation density without any distinct morphology. The SADP shows incomplete rings indicating the presence of very fine recrystallized grains. (c) Higher magnification of (b): The high dislocation density screens the fine grains revealed by the SADP. A few DRX nanograins are arrowed in the micrograph. Note the similarity of morphologies between Figures (6) and (7c), namely high dislocation density and the presence of very fine recrystallized grains (Reprinted from [17]).

Figure 8: A schematic representation of the microstructural refinement as a function of the distance from the ASB/ fracture plane. The microstructure evolves from dislocation cells into subgrains and the density of martensite increases with the proximity to the fracture plane. In the fracture plane an avalanched, high dislocation density area is observed, from which DRX nanograins emanate.

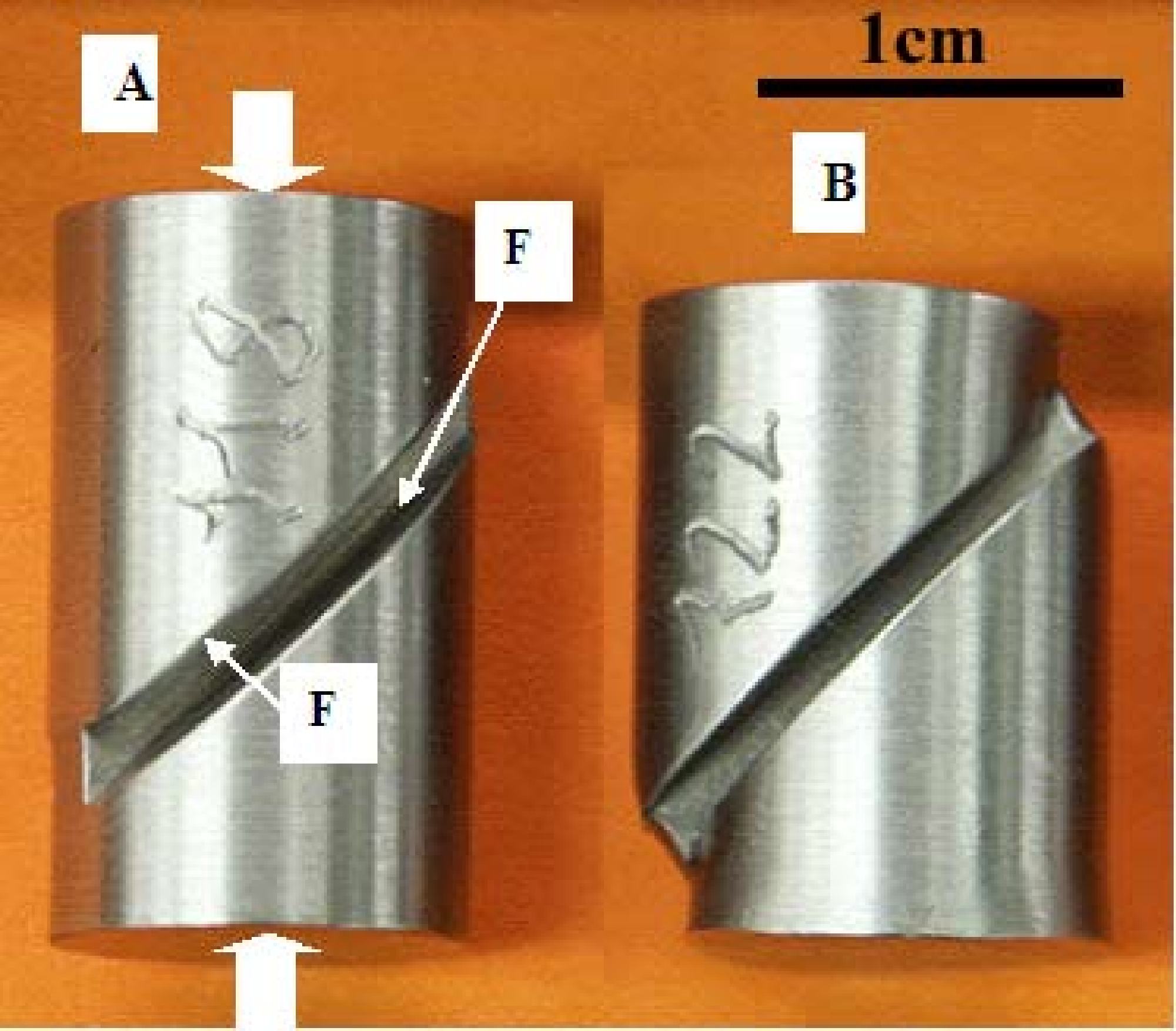
A
F
F
1cm
B

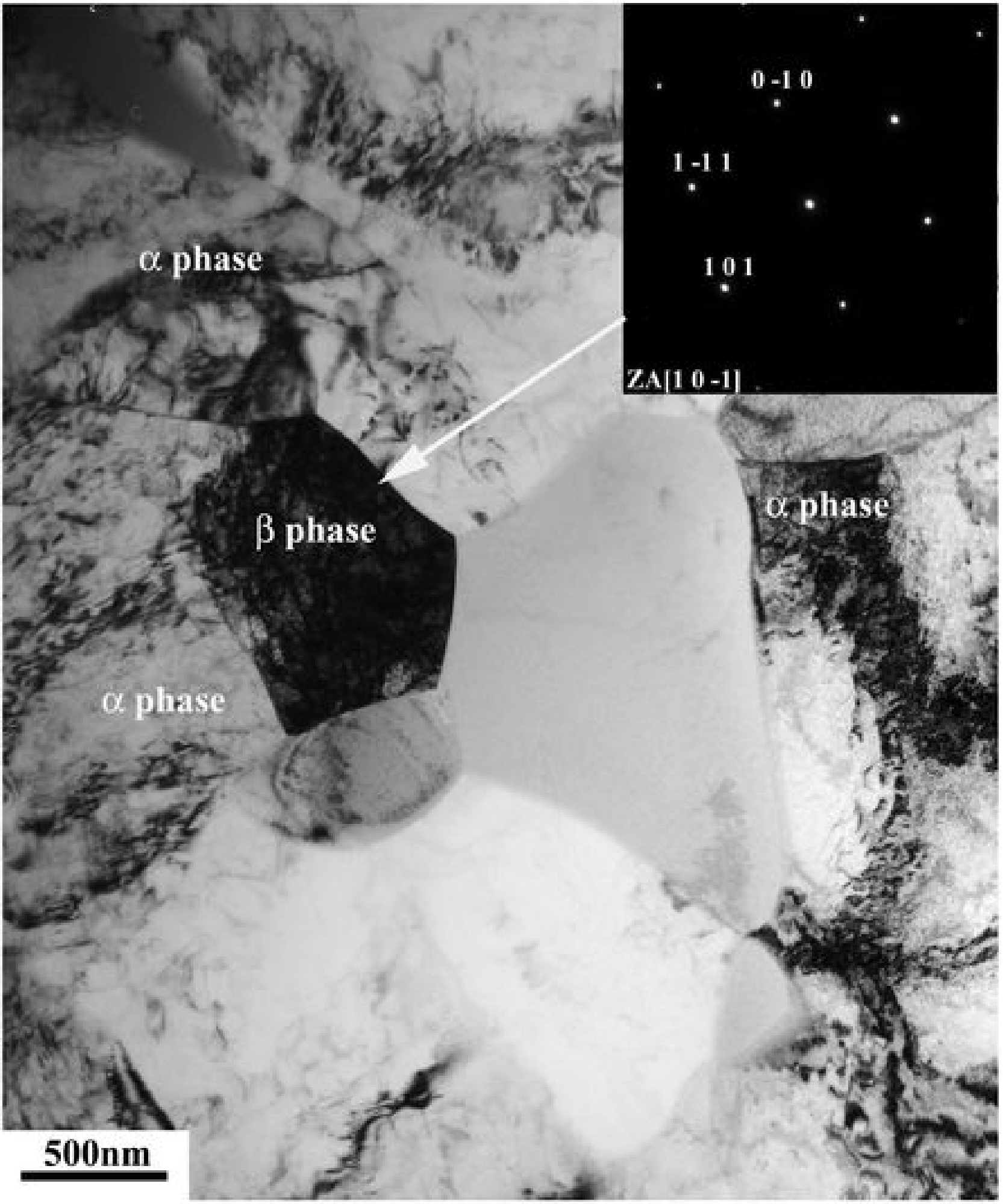
0 -1 0
1 -1 1
1 0 1
ZA[1 0 -1]
α phase
β phase
α phase
α phase
500nm

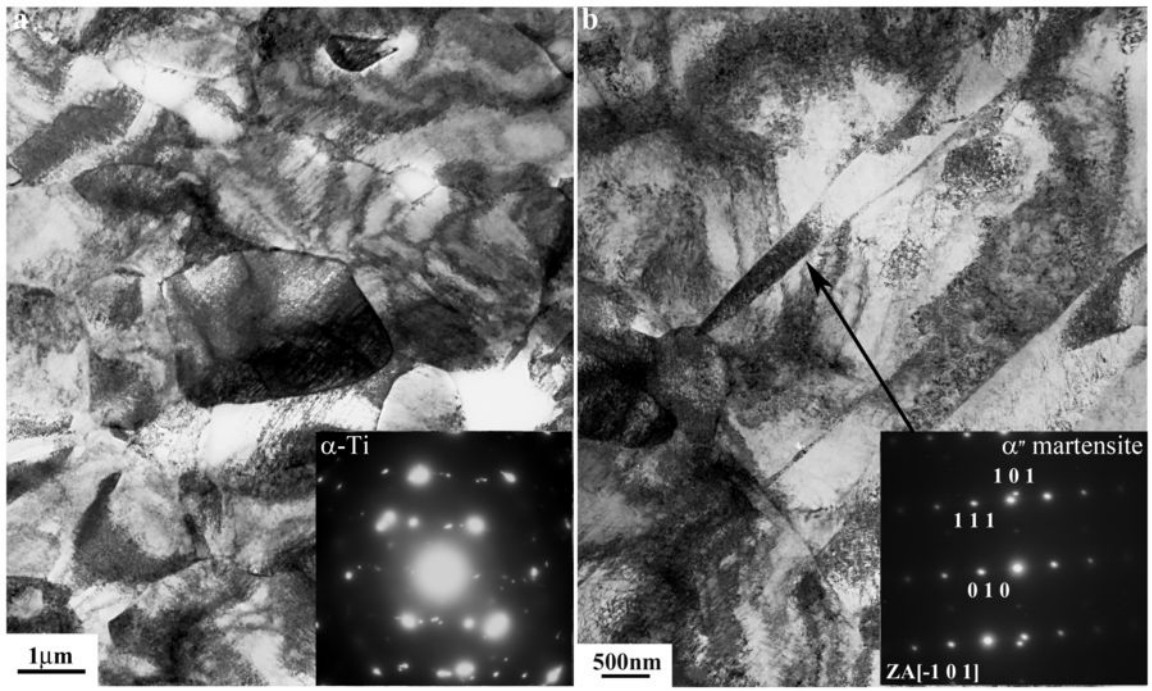
a
α-Ti
1μm
b
α″ martensite
1 0 1
1 1 1
0 1 0
500nm
ZA[-1 0 1]

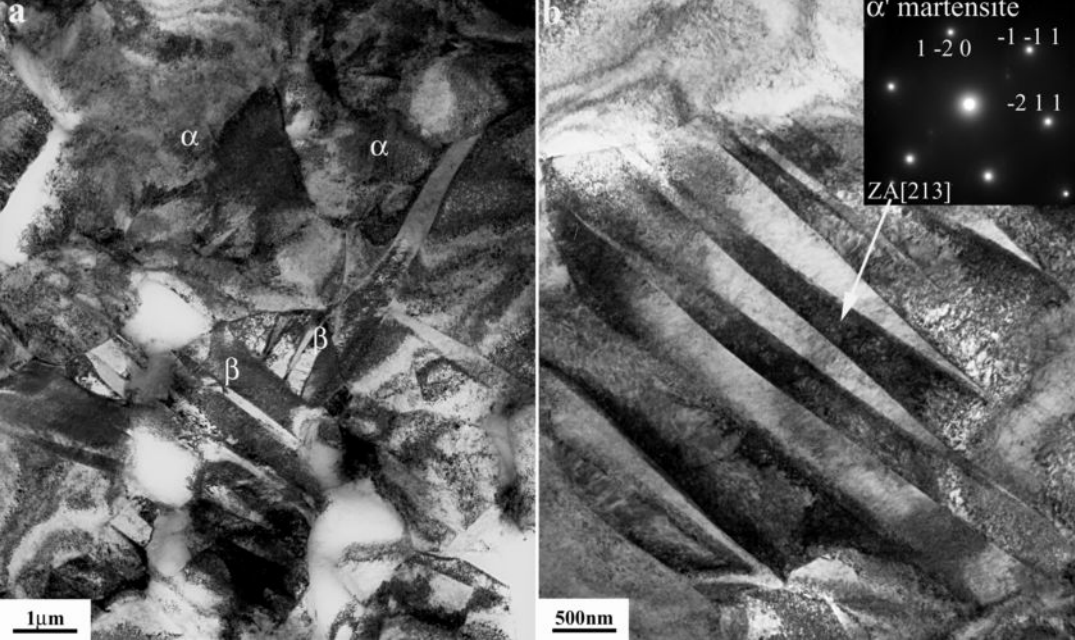
a
α
α
β
β
1μm
b
α' martensite
1 -2 0
-1 -1 1
-2 1 1
ZA[213]
500nm

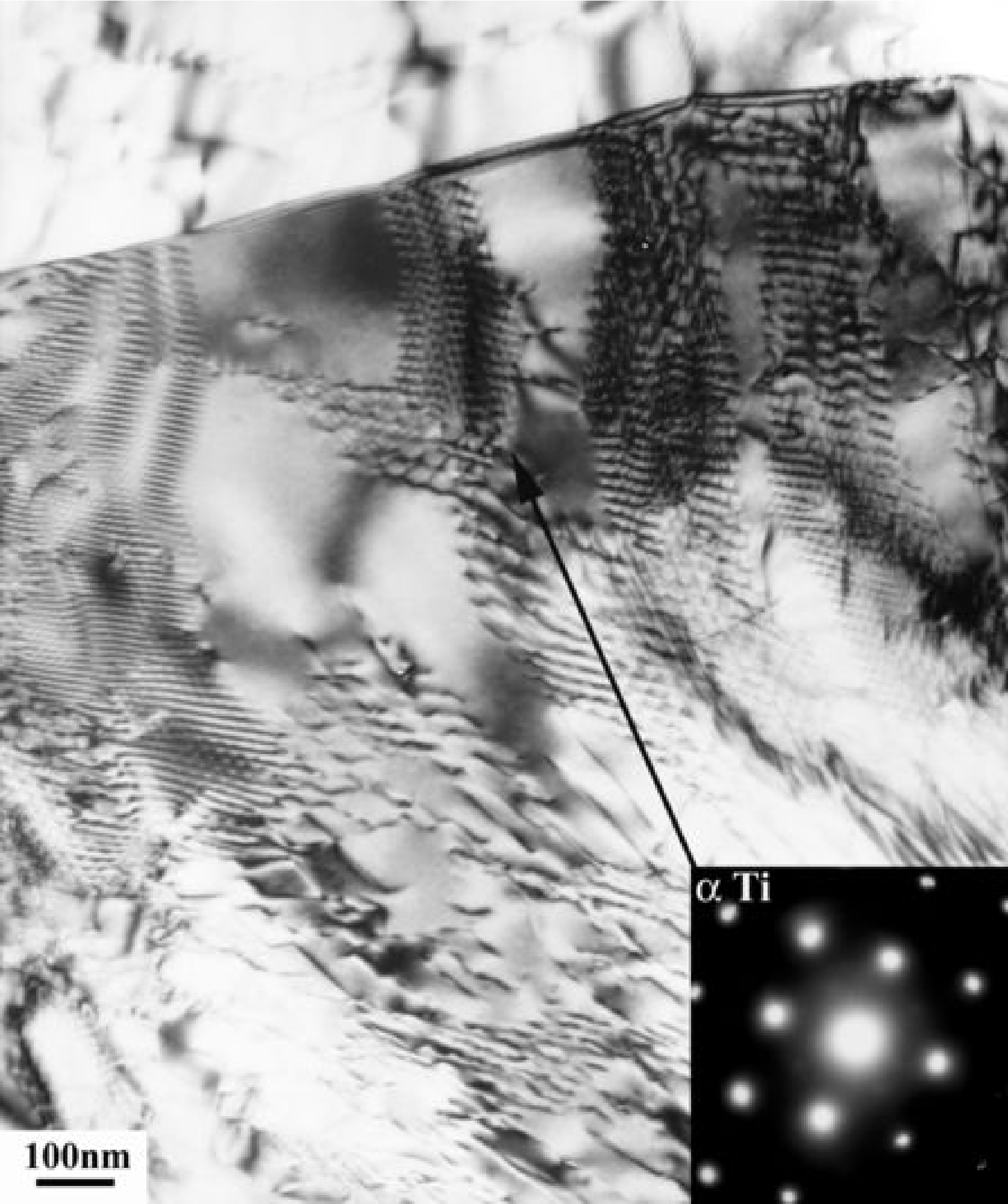
α Ti
100nm

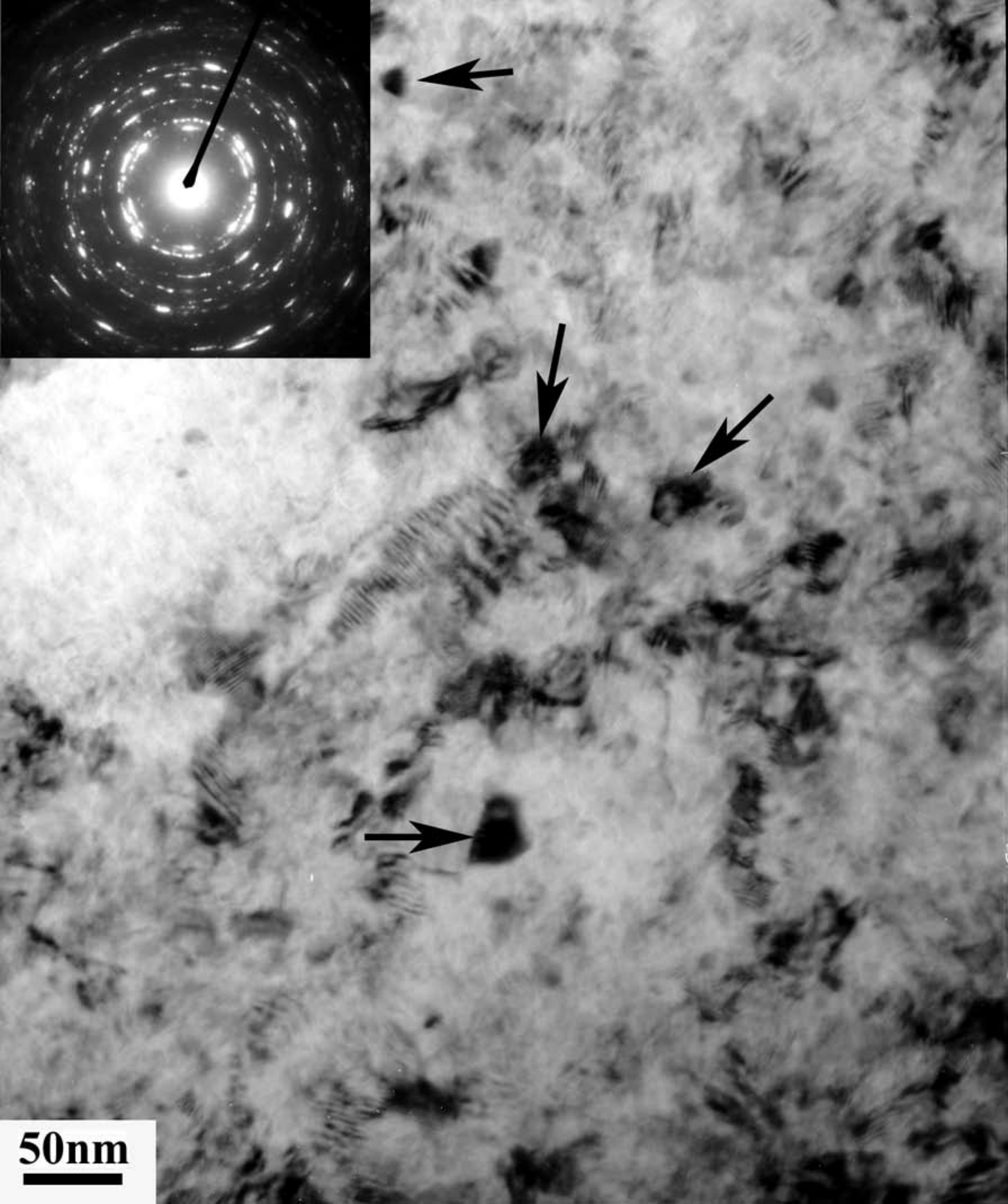
50nm

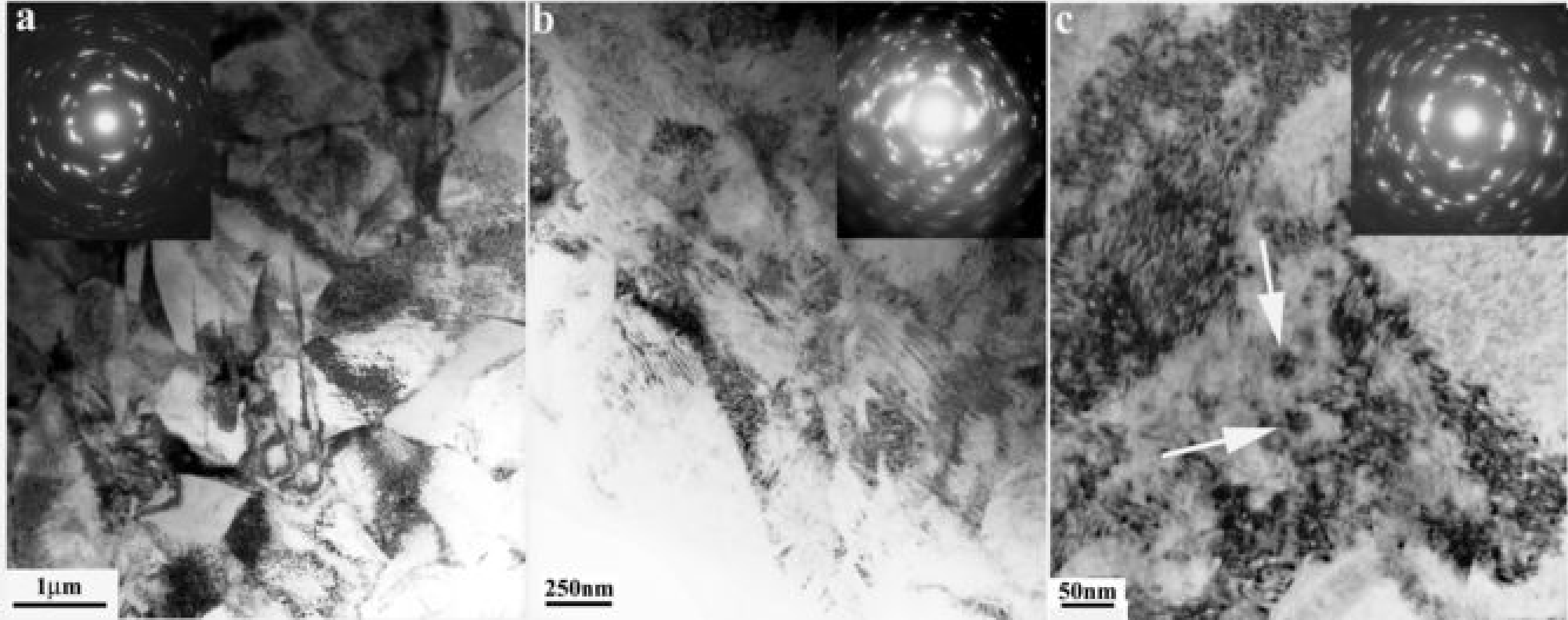
a
1μm
b
250nm
c
50nm

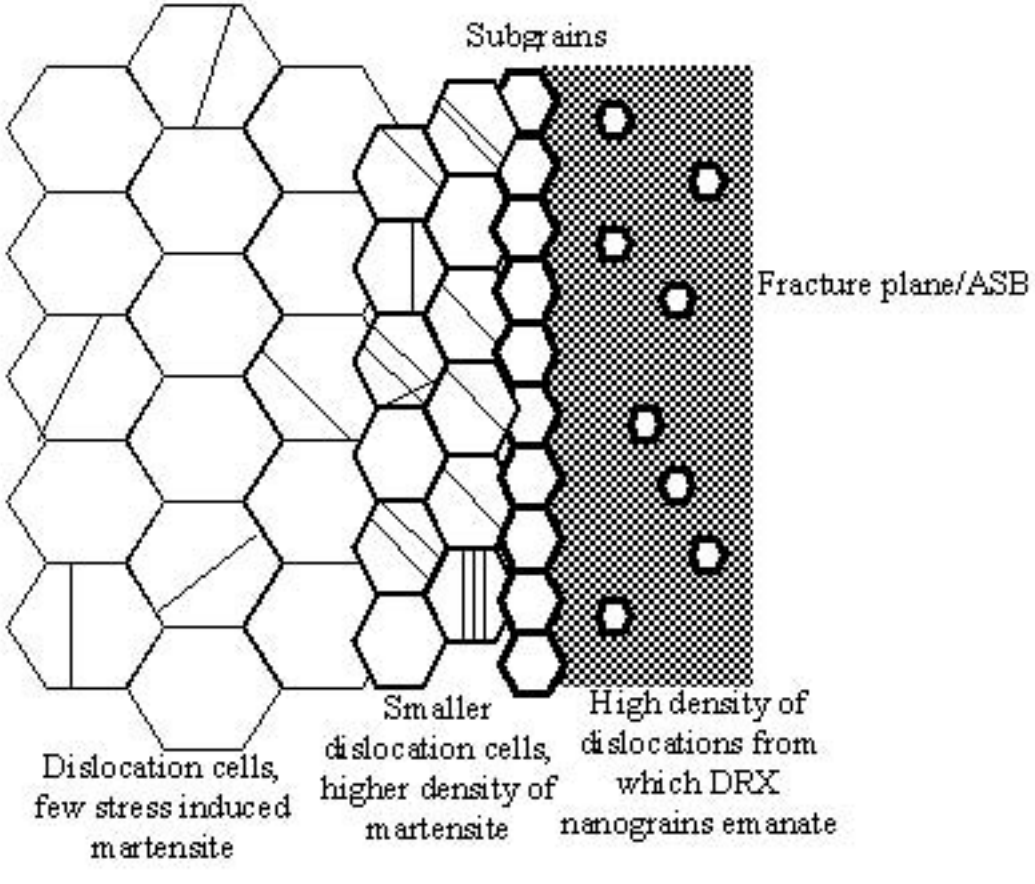
Subgrains
Fracture plane/ASB
Dislocation cells, few stress induced martensite
Smaller dislocation cells, higher density of martensite
High density of dislocations from which DRX nanograins emanate